**LA-UR-24-29632**
**Accepted Manuscript**

# Exploring the relation between transonic dislocation glide and stacking fault width in FCC metals

Jones, Kathryn Rose
Dang, Khanh Quoc
Blaschke, Daniel
Fensin, Saryu Jindal
Hunter, Abigail

Provided by the author(s) and the Los Alamos National Laboratory (1930-01-01).

**To be published in:** Modelling and Simulation in Materials Science and Engineering

**DOI to publisher's version:** 10.1088/1361-651X/adb017

**Permalink to record:**
https://permalink.lanl.gov/object/view?what=info:lanl-repo/lareport/LA-UR-24-29632

Los Alamos NATIONAL LABORATORY

National Nuclear Security Administration

Los Alamos National Laboratory, an affirmative action/equal opportunity employer, is operated by Triad National Security, LLC for the National Nuclear Security Administration of U.S. Department of Energy under contract 89233218CNA000001. By approving this article, the publisher recognizes that the U.S. Government retains nonexclusive, royalty-free license to publish or reproduce the published form of this contribution, or to allow others to do so, for U.S. Government purposes. Los Alamos National Laboratory requests that the publisher identify this article as work performed under the auspices of the U.S. Department of Energy. Los Alamos National Laboratory strongly supports academic freedom and a researcher's right to publish; as an institution, however, the Laboratory does not endorse the viewpoint of a publication or guarantee its technical correctness.

Modelling and
Simulation in Materials
Science and
Engineering

PURPOSE-LED
PUBLISHING™

**PAPER** • **OPEN ACCESS**

# Exploring the relation between transonic dislocation glide and stacking fault width in FCC metals

To cite this article: Kathryn R Jones *et al* 2025 *Modelling Simul. Mater. Sci. Eng.* **33** 025020

View the article online for updates and enhancements.

You may also like

- Mobility of dissociated mixed dislocations under an Escaig stress
Nathaniel Burbery, Raj Das and George Ferguson
- Phonons on the clean metal surfaces and in adsorption structures
G G Rusina and E V Chulkov
- Effect of stacking fault energy on mechanism of plastic deformation in nanotwinned FCC metals
Valery Borovikov, Mikhail I Mendelev, Alexander H King et al.

This content was downloaded from IP address 204.121.192.133 on 18/02/2025 at 21:10

OPEN ACCESS
IOP Publishing
Modelling and Simulation in Materials Science and Engineering
Modelling Simul. Mater. Sci. Eng. **33** (2025) 025020 (14pp) https://doi.org/10.1088/1361-651X/adb017

# Exploring the relation between transonic dislocation glide and stacking fault width in FCC metals

**Kathryn R Jones, Khanh Dang*, Daniel N Blaschke*, Saryu J Fensin and Abigail Hunter**

Los Alamos National Laboratory, Los Alamos, NM 87545, United States of America

E-mail: krjones2@uw.edu, kqdang@lanl.gov, dblaschke@lanl.gov, saryuj@lanl.gov and ahunter@lanl.gov

Received 4 October 2024; revised 20 December 2024
Accepted for publication 23 January 2025
Published 14 February 2025

**Abstract**

Theory predicts limiting gliding velocities that dislocations cannot overcome. Computational and recent experiments have shown that these limiting velocities are soft barriers and dislocations can reach transonic speeds in high rate plastic deformation scenarios. In this paper we systematically examine the mobility of edge and screw dislocations in several face centered cubic (FCC) metals (Al, Au, Pt, and Ni) in the extreme large-applied-stress regime using molecular dynamics simulations. Our results show that edge dislocations are more likely to move at transonic velocities due to their high mobility and lower limiting velocity than screw dislocations. Importantly, among the considered FCC metals, the dislocation core structure determines the dislocation's ability to reach transonic velocities. This is likely due to the variation in stacking fault width due to relativistic effects near the limiting velocities.

Keywords: transonic dislocation glide, stacking fault width, molecular dynamics, FCC metals

* Authors to whom any correspondence should be addressed.

Original Content from this work may be used under the terms of the Creative Commons Attribution 4.0 licence. Any further distribution of this work must maintain attribution to the author(s) and the title of the work, journal citation and DOI.

© 2025 The Author(s). Published by IOP Publishing Ltd

## 1. Introduction

Since its first discovery by Taylor in 1934 [1], dislocation properties have been extensively studied due to their important role in plasticity. However, there are still unresolved questions about dislocation behaviors, especially under extreme loading conditions such as high applied strain rates [2, 3]. In this regime, one of the key questions is whether dislocations can reach transonic and/or supersonic speeds under sufficiently high applied stress. Some early experiments suggested that there may be a limiting velocity of dislocation movement [4, 5]. However, due to the inherent challenges with tracking dislocations in this extreme regime, the first experimental observation of transonic dislocations only happened recently in diamond [6]. Therefore, a majority of the studies of dislocation behaviors in this regime have relied on theoretical and modeling tools such as molecular dynamics (MD) simulations.

Theoretically, the existence of transonic and supersonic dislocations, which are separated from the subsonic ones by critical velocity 'barriers', was predicted by the steady-state theory of perfect dislocations [7, 8]. Importantly, these velocity barriers have been speculated to be soft limits that can be overcome under extreme conditions [9, 10]. This idea was supported by results from MD simulations for face centered cubic (FCC) metals such as Ni, Al, and Cu [10–18], BCC W [19, 20], and HCP Mg [21]. A majority of transonic dislocations are only observed in edge dislocations where the subsonic dislocations asymptotically approach the lowest limiting velocities until some critical stress above which transonic motion becomes possible [10, 11, 14–18, 21]. On the other hand, for screw dislocations, instabilities in the form of additional dislocation nucleation from the existing partials or homogeneously within the simulation box appeared at higher applied shear stresses ($>$500 MPa) in both FCC and HCP metals [10, 12, 17, 21]. In fact, transonic speeds were only observed in Cu screw dislocations at very low temperatures ($<$10 K) [10, 12, 14–17]. It was suggested that at high temperature, the screw dislocations experience larger phonon drag, which prevents them from overcoming the limiting velocities before instabilities occur [10]. However, it remains unclear which parameters govern the ability of one material system's dislocation to reach transonic gliding speeds.

One of the challenges is the lack of a systematic study across different material systems. Dislocation motion via MD simulations can be studied using different simulation setups [12, 14–17, 22]. For instance, there are several methods to apply a shear driving force to move the dislocation such as (i) adding a shear force to the top layer of atoms while fixing the bottom layer of atoms, (ii) applying a shear deformation to the simulation cell, and (iii) applying a velocity to the top layer of atoms to impose a shear strain rate. Moreover, the boundary conditions between fixed versus free boundaries also seem to affect the dislocation mobility at near-sonic velocities [23–25]. Importantly, while there have been MD studies that investigate the behavior of dislocations in the transonic regime [10, 11, 14–18, 21], they used different interatomic potentials and material systems which prevents a comprehensive understanding of which parameter affects the ability of dislocations to accelerate beyond the subsonic regime.

Therefore, the goal of this paper is to explore the governing parameters that control if the dislocation can reach transonic velocities. To achieve this, mobilities of dislocations under high applied shear stresses are systematically investigated in FCC metals such as Al, Au, Pt, and Ni. These material systems and the corresponding interatomic potentials are carefully chosen so that the important dislocation properties such as unstable stacking fault (USF) energy, intrinsic stacking fault (ISF) energy, and shear modulus are varied.

## 2. Methodology: MD simulations

MD simulations are performed using the classical MD simulation code LAMMPS [26] and visualized using the Open Visualization Tool [27]. Table 1 shows the list of interatomic potentials used in this work with important material properties for dislocations such as (average) shear modulus, ISF energy, USF energy, and equilibrium stacking fault widths (SFW) (which were determined for edge dislocations at 0 K). Only FCC metals with the same functional form for the interatomic potentials are used to reduce the complexity of the comparison. For Pt, due to the lack of reasonable embedded atom model (EAM) potentials, a modified EAM is used instead. Importantly, the four FCC material systems and corresponding interatomic potentials are specifically chosen to have a wide range of values for shear modulus, ISF energy, USF energy, and equilibrium SFW.

To model the dislocation mobility, simulation cells with specific orientations are used for edge and screw dislocations as shown in table 2. Table 2 also includes the first two limiting velocities for the edge and screw dislocations. The lowest limiting velocities for these slip systems can be determined analytically by [10, 35]

$$v_{\text{lim}}^{\text{FCC,edge}} = \sqrt{\frac{\min\left(C_{44}, C'\right)}{\rho}}, \qquad v_{\text{lim}}^{\text{FCC,screw}} = \sqrt{\frac{3C'C_{44}}{\rho\left(C_{44}+2C'\right)}}, \tag{1}$$

where $\rho$ denotes the material density and $C' = (C_{11} - C_{12})/2$. The higher limiting velocities were determined numerically as detailed in the review article [35] using the Python code PyDislocDyn [34]. Note that all metals considered in this work have a Zener anisotropy ratio $A = C_{44}/C' > 1$ so that the lowest limiting velocity for edge dislocations depends on $C'$.

The simulation box is approximately $16 \times 52 \times 550$ Å along the $X$, $Y$, and $Z$ directions, respectively. Periodic boundary conditions were applied along the $X$ and $Z$ directions so the dislocation can glide in and out of the simulation box without encountering barriers. Fixed boundary conditions are applied along the $Y$ direction with appropriate pre-strain to alleviate stress caused from thermal expansion. A single dislocation is inserted at the center of the simulation box using the Volterra displacement field with appropriate boundary treatment as detailed in [36, 37]. Shear forces are applied to the top layer atoms to move the dislocations. Once the dislocation motion reaches equilibrium, the dislocation position and SFWs are tracked and determined by using the common neighbor analysis in LAMMPS [26] to identify perfect and defected atoms. While this method is efficient, as temperature and stress increased there were some areas where the lattice shifted enough due to lattice vibrations that it was no longer considered a FCC structure, which complicates the dislocation core region tracking. Data points influenced by this are removed from the analysis. Since the dislocation cores remain planar, only the SFW is used to describe the change in the dislocation core structure. The average velocities and SFWs are recorded only after the dislocation reaches steady state (after 50 ps) for all cases except at 100 K for both edge and screw dislocations in Pt where the full range of data (0 to 300 ps) is included. For these two cases, the dislocation motion transitions into stick-slip behavior instead of steady state glide as seen in figure 1. Understandably, this will slightly overestimate the error for these two cases. Importantly, the averaged velocities do not vary significantly regardless of ranges of recorded data. In order to keep the temperature constant, a Nosé–Hoover type thermostat and barostat were used [38] as described in [37]. This allows slight changes in temperature while still keeping the temperature within a few degrees of the target. Temperature effects are considered by using two temperatures at 10 and 100 K. The applied stresses are increased until the dislocation achieves transonic motion or the simulation exhibits instabilities.

**Table 1.** Potentials of metals used in this work. Three elastic constants were used from the potential file as well as the intrinsic stacking fault (ISF) energy; the shear modulus $G$ was determined by the Kröner average for cubic crystals, see [28]. Density and limiting velocity were calculated using the data from the potential file. The equilibrium SFW was found by running the edge dislocation simulations at a shear stress of 0 MPa and 0 K.

| Metal [Potential] | Lattice constant (Å) | $C_{11}$ (GPa) | $C_{12}$ (GPa) | $C_{44}$ (GPa) | $G$ (GPa) | Intrinsic SFE (mJ m$^{-2}$) | Unstable SFE (mJ m$^{-2}$) | Density (g cm$^{-3}$) | Equilbrium SFW (Å) |
|---|---|---|---|---|---|---|---|---|---|
| Ni [29] | 3.52 | 247.86 | 147.83 | 124.84 | 87.2 | 125.25 | 367.8 | 8.94 | 31.37 |
| Pt [30] | 3.92 | 358.12 | 253.51 | 77.55 | 66.4 | 110 | 596.0 [31] | 21.55 | 16.20 |
| Au [32] | 4.07 | 201.65 | 169.53 | 45.97 | 30.8 | 42.58 | 91.69 | 19.4 | 67.04 |
| Al [33] | 4.05 | 116.82 | 60.12 | 31.66 | 30.3 | 113.77 | 149.72 | 2.70 | 22.55 |

**Table 2.** Crystal lattice orientation in the $X$, $Y$ and $Z$ direction for edge and screw dislocations as well as the limiting velocities for each metal and type of dislocation, calculated using [34], see also [35].

| Metal | Dislocation type | $X$ | $Y$ | $Z$ | 1st limiting velocity (km s$^{-1}$) | 2nd limiting velocity (km s$^{-1}$) |
|---|---|---|---|---|---|---|
| Ni | Edge | $[1\bar{2}1]$ | [111] | $[\bar{1}01]$ | 2.37 | 3.74 |
| | Screw | $[\bar{1}01]$ | [111] | $[\bar{1}2\bar{1}]$ | 3.05 | N/A |
| Pt | Edge | $[1\bar{2}1]$ | [111] | $[\bar{1}01]$ | 1.55 | 1.90 |
| | Screw | $[\bar{1}01]$ | [111] | $[\bar{1}2\bar{1}]$ | 1.76 | N/A |
| Au | Edge | $[1\bar{2}1]$ | [111] | $[\bar{1}01]$ | 0.91 | 1.54 |
| | Screw | $[\bar{1}01]$ | [111] | $[\bar{1}2\bar{1}]$ | 1.21 | N/A |
| Al | Edge | $[1\bar{2}1]$ | [111] | $[\bar{1}01]$ | 3.24 | 3.42 |
| | Screw | $[\bar{1}01]$ | [111] | $[\bar{1}2\bar{1}]$ | 3.36 | N/A |

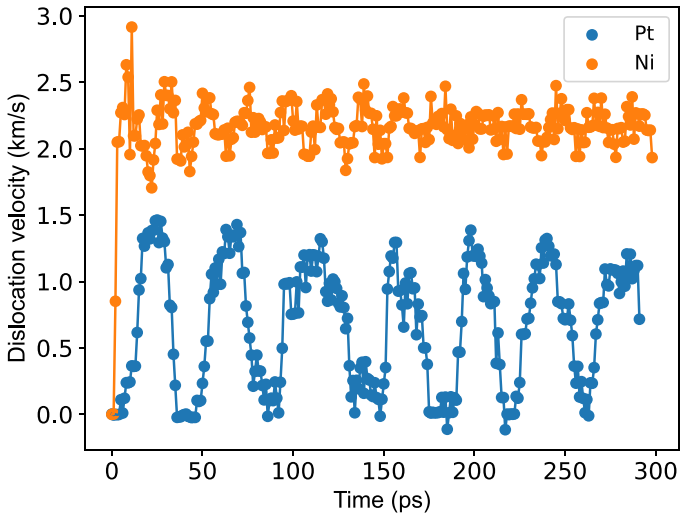


**Figure 1.** We highlight the difference in edge dislocation motion between Ni, where dislocation glide quickly converges to an (almost) steady state, and Pt, which exhibits a 'stick-slip' behavior.

## 3. Results

### *3.1. Mobility of screw dislocations*

Figures 2(a)–(d) show the mobility curves for screw dislocations in Al, Ni, Au, and Pt. Compared to Ni and Al, Au and Pt dislocations are less mobile. The lower mobilities of Au could be due to the relatively lower ISF energy and thus larger dislocation core structures compared to Al and Ni [39]. Among the four, Pt dislocations are extremely immobile with dislocation glide observed only for applied stress greater than 2.25 GPa at 10 K and greater than 1.5 GPa at 100 K. The significantly higher Peierls stress of Pt dislocations could be due to

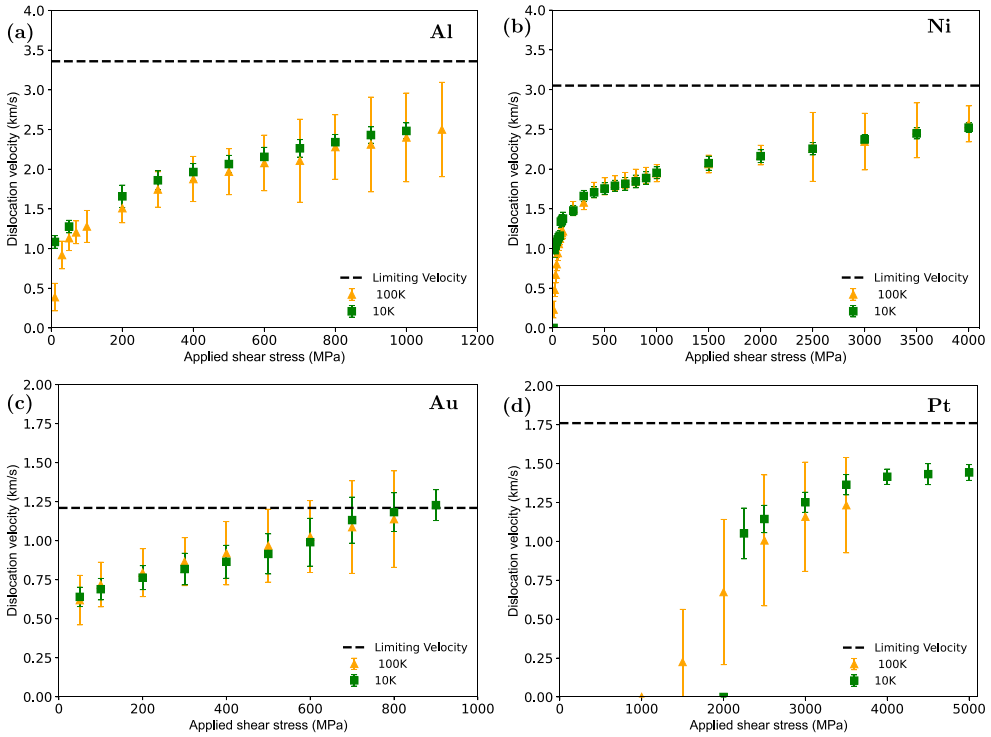


**Figure 2.** Velocity of screw dislocations in Al (a), Ni (b), Au (c) and Pt (d) vs the shear stress applied. The dashed lines indicate the limiting velocities.

the combination of high shear modulus (shown in table 1) and small equilibrium SFW according to the analytical Peierls-Nabarro model. For the same applied shear stress, the dislocation velocities at higher temperature (100 K) also fluctuate more compared to the ones at 10 K.

For each material, the mobility curve contains two distinct regimes of phonon and radiative drag. As the applied stress increases, the dislocation velocities start to plateau below the limiting velocities shown in table 2. Higher applied shear stresses result in nucleation of additional dislocations or defects that prevent the proper tracking and determination of dislocation velocities, and thus these simulations are not included in the analysis. Importantly, no transonic jump is observed for screw dislocations, though the highest screw dislocation velocity observed in Au at 10 K barely exceeds the calculated limiting velocity (which is within the error bars). For the other three FCC metals, no transonic dislocations are found. This result is consistent with previous MD simulations for screw dislocations where only transonic dislocation motion is observed in Cu at very low temperature ($<$10 K) [35].

### *3.2. Mobility of edge dislocations*

Figure 3 shows the mobility curves for edge dislocations in Al, Ni, Au, and Pt. Overall, edge dislocations for all considered FCC metals are more mobile than screw dislocations. Similar to screw dislocations, the mobility of edge dislocations also scale linearly with applied shear stress at low velocities and eventually plateau at or near the limiting velocities as the stress increases. However, unlike screw dislocations, transonic and supersonic velocities are

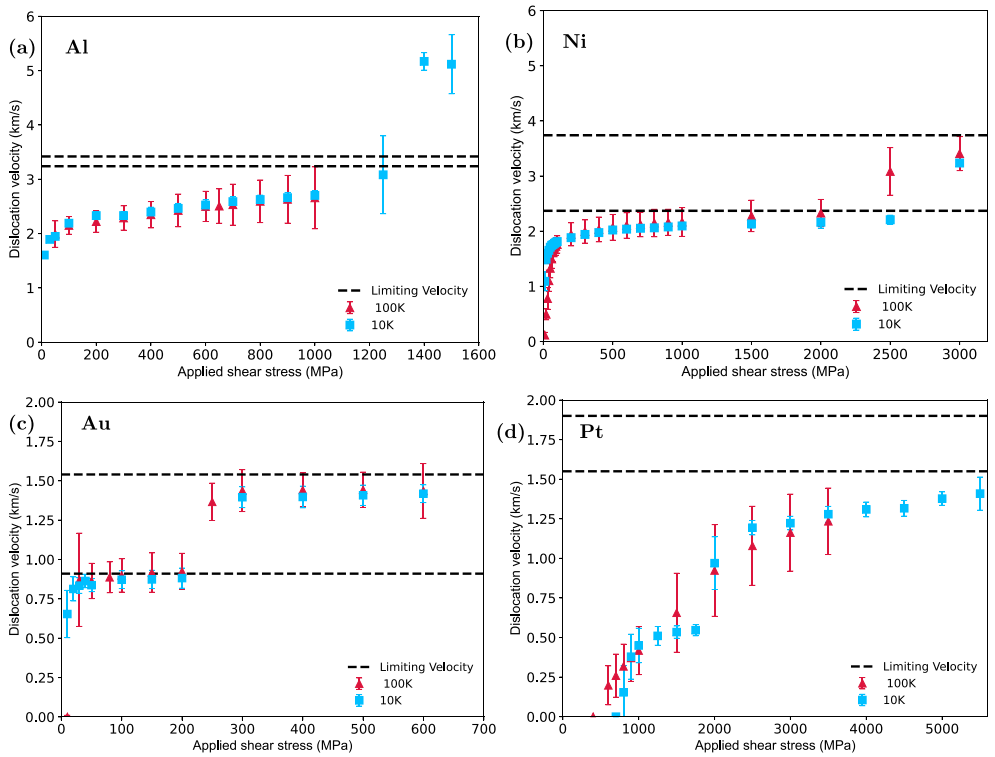


**Figure 3.** Velocity of edge dislocations in Al (a), Ni (b), Au (c) and Pt (d) vs the shear stress applied. The dashed lines indicate the two lowest limiting velocities.

observed in edge dislocations for large applied shear stresses. For Al, there is a jump in the dislocation velocity to the (second) transonic regime at 10 K with applied shear stress of 1.3 GPa, but there was no jump at 100 K. In contrast to Au and Ni discussed below, the first transonic regime is skipped, possibly due to to the first two limiting velocities being in close proximity of one another. At 100 K, additional dislocations start to form, glide, and interact with the existing edge dislocation. This is different from previous MD simulations by Olmsted *et al* [12] where the authors observed transonic speed of edge dislocations in Al at higher temperature ($>$ 324 K). This is due to the difference in the utilized interatomic potentials between the two studies. As shown in figure 3, Au and Pt edge dislocations have a lower mobility compared to Al and Ni ones. Both reach velocities of approximately 1.4 km s$^{-1}$ compared to 5 and 3.24 km s$^{-1}$ for Al and Ni dislocations, respectively. In particular, Pt dislocations are less mobile compared to the other three materials and only start gliding with applied shear stress above 600 and 300 MPa at 10 and 100 K, respectively. Importantly, even though the Pt edge dislocation is much more mobile compared to its screw counterpart, it also does not reach transonic velocity even at extremely high applied shear stress of 5 GPa. Above this shear stress, instabilities occur via nucleation of additional dislocations. On the other hand, the Au edge dislocation does not only cross over the 1st limiting velocity at applied shear stress greater than 200 MPa but also comes close to the 2nd limiting velocity.

In order to understand the behavior of the dislocation core structure as the dislocations reach the limiting velocities, figures 4(a) and (b) show the mobility curves and SFWs of Al

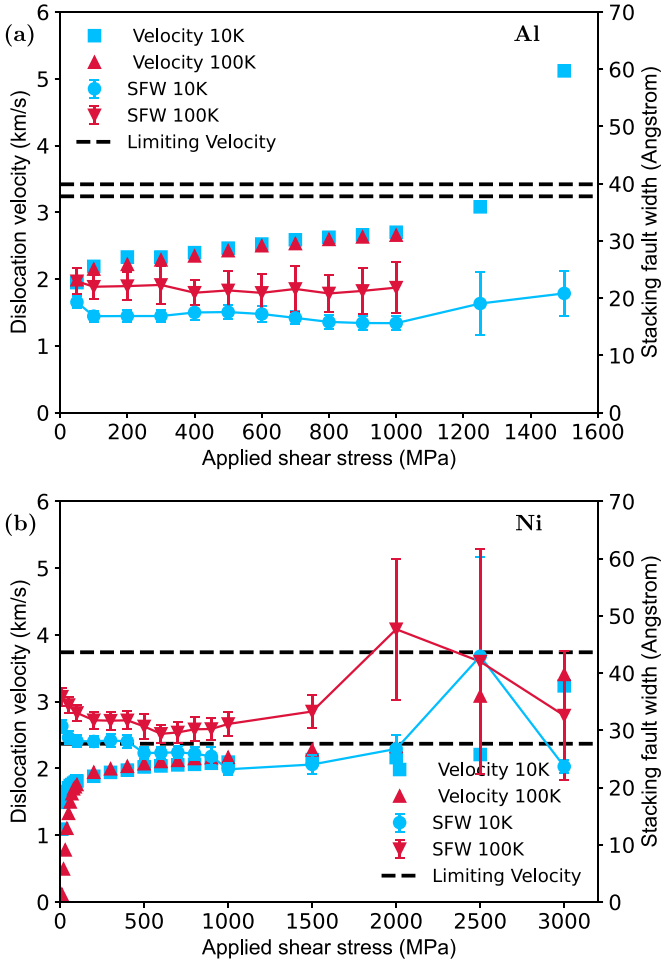


**Figure 4.** Velocity and stacking fault width of edge dislocations in Al (a) and Ni (b) vs the shear stress applied. The dashed lines indicate the two lowest limiting velocities.

and Ni edge dislocations, respectively. Initially, the SFW of the Al edge dislocations slightly reduce until the dislocation velocities reach approximately 2.7 km s$^{-1}$. At 1.25 GPa applied shear stress where the dislocation jumps to the transonic regime, the SFW slightly increases. For Ni, the dislocation velocity jumps to the transonic regime (at about 3.27 km s$^{-1}$) at an applied shear stress of 2 GPa and 2.5 GPa for temperatures of 10 and 100 K, respectively, as shown in figure 4(b). The transonic dislocation motion is consistent with previous MD results for edge dislocations in Ni using a different EAM potential [12]. The dislocation velocity jump happens at a lower stress for higher temperatures which could be due to the larger dislocation core as the temperature increases [40, 41]. Similar to Al, the Ni edge dislocation also reduces its SFW at first up to the velocity of about 2.09 km s$^{-1}$. From there, the SFW increases as the dislocation gets closer to the limiting velocities. However, unlike Al, once the dislocation reaches transonic speed, its SFW contracts. As they transition into the transonic regime, Ni

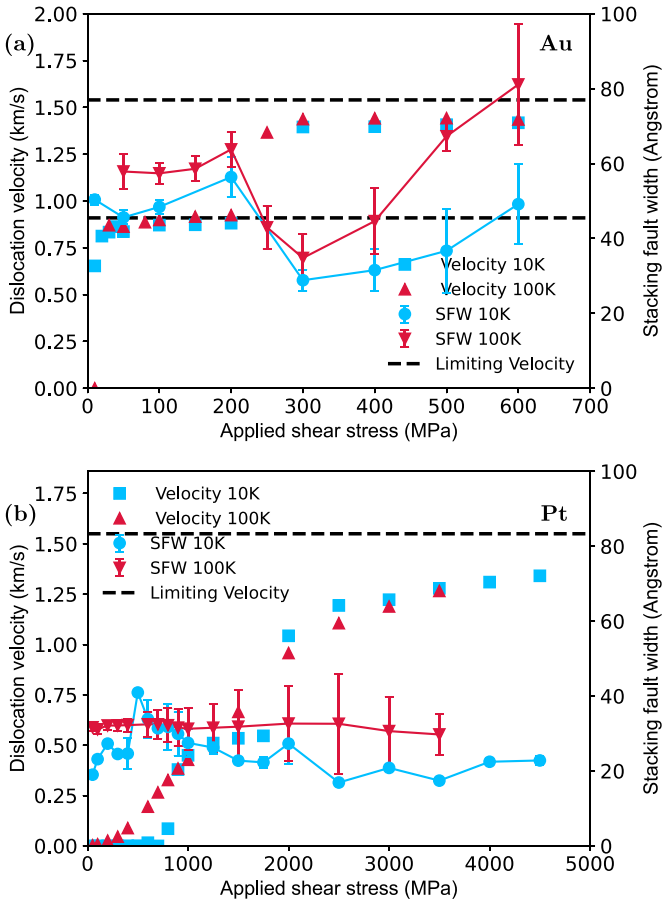


**Figure 5.** Velocity of edge dislocations in Au (a) and Pt (b) vs the shear stress applied. The dashed lines indicate the (lowest) limiting velocities.

edge dislocations also contract and extend more during their glide motions compared to the Al edge dislocations, which results in higher standard deviations in SFWs shown in figure 4.

Similarly, figure 5 shows the mobility curves and SFWs of Au and Pt edge dislocations, respectively. For Pt edge dislocations, the SFW at 100 K remains relatively constant. At a lower temperature of 10 K, the SFW increases up to an applied shear stress of 600 MPa, where the edge dislocation starts to move. Then, the SFW reduces back to the previous values and remains constant as the applied shear stress increases. On the other hand, the SFW of Au edge dislocations at both 10 K and 100 K reduces initially, then increases as the velocities approaches the 1st limiting velocity of 0.91 km $s^{-1}$. As the dislocation velocities cross over this limiting velocity, the SFW reduces again until the applied shear stress approaches 300 MPa. For applied shear stresses greater than 300 MPa, the Au edge dislocation core starts to widen again as its velocity approaches the 2nd limiting velocity of 1.54 km $s^{-1}$. The expansion and constriction of the SFW for moving dislocations at different velocities is likely due to the interplay between dislocation drag and relativistic effects [42–44].

In closing, we note that the SFW of the screw dislocations look similar, i.e. slight initial contraction and subsequent hint of expansion (not shown), with the main exception that there is no contraction at very high stress, consistent with the absence of any transonic screw dislocation velocity.

## 4. Discussion

### *4.1. Variations in dislocation SFW as the velocity becomes transonic*

The evolution of the SFWs seen in this study as the edge dislocations glide with subsonic to transonic velocities can be explained by the relativistic effects on dislocation core structures. Specifically, the relativistic effect influences the dislocation core structure when the dislocation velocity approaches the limiting velocities, similar to Einstein's theory of relativity for particles approaching the speed of light [42, 45]. As the speed increases up to the Rayleigh wave speed, the interaction force between the screw components decreases while it increases for the edge components. Hirth and Lothe determined the SFWs between partials in FCC and BCC metals via a Lagrangian formulation. They found that a screw dislocation core in FCC metals would constrict with increasing speed until it reaches 80% the transverse sound speed where the trend is reversed and the dislocation core widens and eventually splits apart at the transverse sound speed [46]. For dissociated edge dislocations approaching the Rayleigh wave speed, the attractive force between the opposite sign screw components will decrease and the repulsive force between the same signed edge components will increase [47]. This leads to the extension of the SFW as the speed approaches the Rayleigh wave and limiting speed. Once the dislocation's speed surpasses the limiting velocities, this relativistic effect is removed. As a result, the dissociated edge dislocations constrict as seen in figures 4 and 5 for Ni and Au, respectively. For Au, the SFW expands again once the dislocation's velocity approaches the 2nd limiting velocity. To the authors' knowledge, this is the first validation of the relativistic effects on edge dislocation core structure that was previously proposed in theory [46, 47].

### *4.2. Governing parameters for transonic dislocation motion*

The MD results in this work show certain trends for transonic dislocation motion behavior:

1. Transonic motion is more frequently observed for edge dislocations than screw dislocations, which is consistent with previous MD simulation studies [12, 17, 21].
2. Transonic motion is more frequently observed for FCC metals with large SFWs.

These two results can be rationalized by understanding how transonic motion can be achieved. There are three intertwined factors that control this process: drag coefficient, instability, and limiting velocities, which depend on material properties such as stacking fault energies and elastic constants. For example, the drag coefficient is sensitive to the shear modulus [48]. The instability caused by nucleation of additional dislocations depends on the USF energy. Finally, limiting velocities have been shown in previous studies [35] to be dependent on the elastic constants. However, it is most important to note that any unfavorable values of these parameters can prevent the transonic motion of dislocations. For instance, a favorable drag coefficient and low limiting velocities can still fail to achieve dislocation transonic motion if the stress for instabilities to occur is too low (i.e. before the stress required for transonic motion can be reached).

Based on these three parameters, the first trend can be explained. For FCC metals, screw dislocations tend to have higher limiting velocities (see table 2) but lower mobilities than edge dislocations. This indicates a lower driving force and lower required target velocity for edge dislocations to achieve transonic motion compared to screw dislocations. Note that while it is more challenging for screw dislocations to achieve transonic motion, it is still possible. For example, transonic screw dislocations have been observed in Cu [10] at low temperature. In this study, a low-temperature Au screw dislocation also approached the limiting velocity within 1%.

For the second trend, the effects of SFWs on the feasibility of dislocations to achieve transonic motion is clearly shown in this work. Specifically, Pt edge dislocations, with the smallest equilibrium SFW as shown in table 1, do not reach transonic velocities. Similarly, Al edge dislocations, with the 2nd smallest equilibrium SFW, only reach transonic velocity at low temperatures (namely 10 K). On the other hand, Au and Ni edge dislocations with larger equilibrium SFWs both reach transonic velocities at both 10 and 100 K. Small SFWs are equivalent to large ISF and USF energies as shown in previous studies [37, 49, 50] where the dislocation core width is roughly inversely proportional to the product between these two stacking fault energies divided by the (averaged) shear modulus $G$. With these large stacking fault energies, it is likely that the small SFWs in Pt dislocations (and Al dislocations to some extent) are less likely to expand when approaching the limiting velocities, which prevents them from crossing over to the transonic regime. Overall, a material system's ability to achieve transonic dislocation velocity seems to depend on the interplay of the (slip system dependent) effective shear modulus (i.e. lowest limiting velocity), as well as the SFW, ISF, and USF energies.

Predicting where and when the dislocations cross over to the transonic regime remains challenging. Figure 6 shows the transition stresses, which are the lowest stress for the dislocations to move at velocities greater than a limiting velocity, at 100 K and corresponding material properties/parameters. MD simulation data from [12] for Ni (100 K) and Al (216 K) as well as [17] for Cu (10 K) are also included. While the transition stress for FCC edge dislocations is generally proportional to both the $C' = (C_{11} - C_{12})/2$ (which controls their lowest limiting velocity for the metals discussed here) and the USF energy (which is known to affect dislocation mobility, see [51] and references therein), there was not a clear relationship between them. One can argue that higher temperatures make it easier to reach transonic gliding velocities, so that the 216 K and 100 K data points (i.e. the lowest reported temperatures for Al and Ni in [12]) would move to the right if the temperature was reduced to 10 K. This would lead to better agreement with the linear trend of figure 6(a) and with our own simulation data at 10 K (except for one outlier, Cu of [17]). Attempts to connect to other parameters also provide no clear trends with the transition stresses. This is to be expected since the transonic dislocation motion relies on the interplay between three parameters as mentioned earlier.

## 5. Conclusions

In conclusion, the transonic motion of dislocations in FCC metals are systematically studied using MD simulations of edge and screw dislocations. It was found that transonic velocities are easier to achieve by edge dislocations compared to screw dislocations due to their higher mobilities and lower limiting velocities. Moreover, the dislocation core is found to widen as the edge dislocation approaches the limiting velocities and constrict again once the dislocation reaches the transonic velocity, which is due to the relativistic effects. Importantly, it is also found that the dislocation's ability to reach transonic velocities is proportional to its SFW.

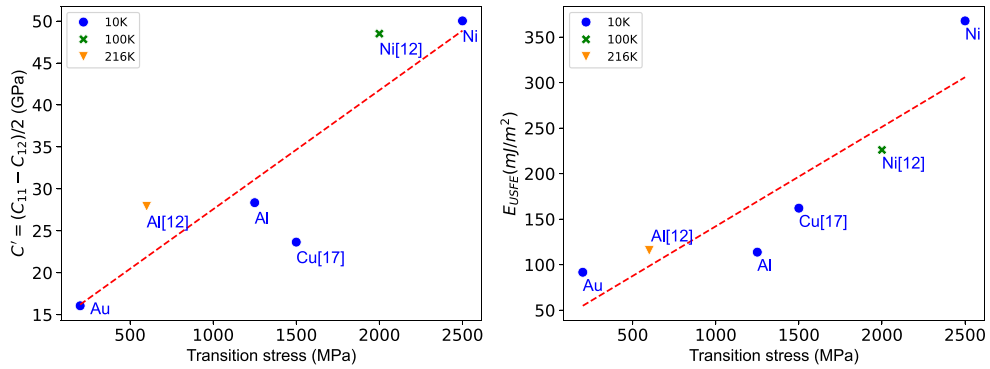


**Figure 6.** $C' = (C_{11} - C_{12})/2$ elastic constant (a) and unstable stacking fault (USF) energy (b) for different transition stresses of FCC metals in this study and previous MD simulation studies [12, 17]. Elastic constants are given for 0 K whereas the transition stress was determined at the temperatures indicated in the figure labels.

While this study only focuses on FCC metals, these results highlight the importance of the dislocation core structure to dislocation mobility in the extreme regime.

## Data availability statement

The data that support the findings of this study are available upon reasonable request from the authors.

## Acknowledgment

We thank the two reviewers for numerous helpful comments. This work was supported by the Advanced Technology Development and Mitigation (ATDM) project and the Physics and Engineering Models (PEM) Materials project within the Advanced Simulation and Computing (ASC) Program of the U.S. Department of Energy under contract 89233218CNA000001. This research used resources provided by the Los Alamos National Laboratory Institutional Computing Program, which is supported by the U.S. Department of Energy National Nuclear Security Administration under Contract No. 89233218CNA000001.

## ORCID iDs

Kathryn R Jones https://orcid.org/0009-0006-1034-1695
Khanh Dang https://orcid.org/0000-0002-9686-4270
Daniel N Blaschke https://orcid.org/0000-0001-5138-1462
Saryu J Fensin https://orcid.org/0000-0001-8135-5353
Abigail Hunter https://orcid.org/0000-0002-0443-4020

## References

[1] Taylor G I 1934 The mechanism of plastic deformation of crystals. Part I.—Theoretical *Proc. R. Soc.* A **145** 362–87

[2] Gurrutxaga-Lerma B, Verschueren J, Sutton A P and Dini D 2021 The mechanics and physics of high-speed dislocations: a critical review *Int. Mater. Rev.* **66** 215–55
[3] Pellegrini Y-P and Josien M 2023 Shock-driven nucleation and self-organization of dislocations in the dynamical Peierls model *Phys. Rev.* B **108** 054309
[4] Parameswaran V R and Weertman J 1971 Dislocation mobility in lead and Pb-In alloy single crystals *Metall. Trans.* **2** 1543–916
[5] Weertman J, Vreeland T and Jassby K M 1973 *Dislocation Mechanics at High Strain Rates* (Springer) pp 319–33
[6] Katagiri K *et al* 2023 Transonic dislocation propagation in diamond *Science* **382** 69–72
[7] Weertman J 1981 Moving dislocations in a shock front *Shock Waves and High-Strain-Rate Phenomena in Metals: Concepts and Applications* (Springer) pp 469–86
[8] Rosakis P 2001 Supersonic dislocation kinetics from an augmented Peierls model *Phys. Rev. Lett.* **86** 95–98
[9] Markenscoff X and Huang S 2008 Analysis for a screw dislocation accelerating through the shear-wave speed barrier *J. Mech. Phys. Solids* **56** 2225–39
[10] Blaschke D N, Chen J, Fensin S and Szajewski B A 2021 Clarifying the definition of 'transonic' screw dislocations *Phil. Mag.* **101** 997–1018
[11] Groh S, Marin E B, Horstemeyer M F and Bammann D J 2009 Dislocation motion in magnesium: a study by molecular statics and molecular dynamics *Modelling Simul. Mater. Sci. Eng.* **17** 075009
[12] Olmsted D L, Hector Jr L G, Curtin W A and Clifton R J 2005 Atomistic simulations of dislocation mobility in Al, Ni and Al/Mg alloys *Modelling Simul. Mater. Sci. Eng.* **13** 371–88
[13] Daphalapurkar N, Wilkerson J, Wright T and Ramesh K 2014 Kinetics of a fast moving twin boundary in nickel *Acta Mater.* **68** 82–92
[14] Marian J and Caro A 2006 Moving dislocations in disordered alloys: connecting continuum and discrete models with atomistic simulations *Phys. Rev.* B **74** 024113
[15] Tsuzuki H, Branicio P S and Rino J P 2009 Molecular dynamics simulation of fast dislocations in copper *Acta Mater.* **57** 1843–55
[16] Peng S, Wei Y, Jin Z and Yang W 2019 Supersonic screw dislocations gliding at the shear wave speed *Phys. Rev. Lett.* **122** 045501
[17] Oren E, Yahel E and Makov G 2016 Dislocation kinematics: a molecular dynamics study in Cu *Modelling Simul. Mater. Sci. Eng.* **25** 025002
[18] Young Vandersall J A and Wirth B D 2004 Supersonic dislocation stability and nano-twin formation at high strain rate *Phil. Mag.* **84** 3755–69
[19] Gumbsch P and Gao H 1999 Dislocations faster than the speed of sound *Science* **283** 965–8
[20] Li Q and Shi S-Q 2002 Dislocation jumping over the sound barrier in tungsten *Appl. Phys. Lett.* **80** 3069–71
[21] Dang K, Blaschke D N, Fensin S and Luscher D J 2022 Limiting velocities and transonic dislocations in Mg *Comput. Mater. Sci.* **215** 111786
[22] Bertin N, Sills R B and Cai W 2020 Frontiers in the simulation of dislocations *Annu. Rev. Mater. Res.* **50** 437–64
[23] Duong T and Demkowicz M J 2023 Resonance with surface waves induces forbidden velocity bands in dislocation glide *J. Mech. Phys. Solids* **180** 105422
[24] Duong T, Dingreville R and Demkowicz M J 2024 Mobility of twinning dislocations in copper up to supersonic speeds *Acta Mater.* **275** 120050
[25] Blaschke D N, Duong T and Demkowicz M J 2023 Comparing theoretical predictions of radiation-free velocities of edge dislocations to molecular dynamics simulations *Phys. Rev.* B **108** 224102
[26] Thompson A P *et al* 2022 LAMMPS - a flexible simulation tool for particle-based materials modeling at the atomic, meso and continuum scales *Comput. Phys. Commun.* **271** 108171
[27] Stukowski A 2010 Visualization and analysis of atomistic simulation data with OVITO-the open visualization tool *Modelling Simul. Mater. Sci. Eng.* **18** 015012
[28] Blaschke D N 2017 Averaging of elastic constants for polycrystals *J. Appl. Phys.* **122** 145110
[29] Mishin Y, Farkas D, Mehl M J and Papaconstantopoulos D A 1999 Interatomic potentials for monoatomic metals from experimental data and ab initio calculations *Phys. Rev.* B **59** 3393–407
[30] Lee B-J, Shim J-H and Baskes M I 2003 Semiempirical atomic potentials for the fcc metals Cu, Ag, Au, Ni, Pd, Pt, Al and Pb based on first and second nearest-neighbor modified embedded atom method *Phys. Rev.* B **68** 144112

[31] Wei X-M, Zhang J-M and Xu K-W 2007 Generalized stacking fault energy in FCC metals with MEAM *Appl. Surf. Sci.* **254** 1489–92
[32] Grochola G, Russo S P and Snook I K 2005 On fitting a gold embedded atom method potential using the force matching method *J. Chem. Phys.* **123** 204719
[33] Zope R R and Mishin Y 2003 Interatomic potentials for atomistic simulations of the Ti-Al system *Phys. Rev.* B **68** 024102
[34] Blaschke D N 2018–2024 PyDislocDyn Computer Software (available at: https://doi.org/10.11578/dc.20180619.15)
[35] Blaschke D N 2021 How to determine limiting velocities of dislocations in anisotropic crystals *J. Phys.: Condens. Matter* **33** 503005
[36] Dang K and Spearot D 2018 Pressure dependence of the Peierls stress in aluminum *JOM* **70** 1094–9
[37] Dang K, Bamney D, Bootsita K, Capolungo L and Spearot D E 2019 Mobility of dislocations in aluminum: faceting and asymmetry during nanoscale dislocation shear loop expansion *Acta Mater.* **168** 426–35
[38] Melchionna S, Ciccotti G and Holian B L 1993 Hoover NPT dynamics for systems varying in shape and size *Mol. Phys.* **78** 533–44
[39] Mills M and Neeraj T 2001 Dislocations in metals and metallic alloys *Encyclopedia of Materials: Science and Technology* ed K J Buschow, R W Cahn, M C Flemings, B Ilschner, E J Kramer, S Mahajan and P Veyssière (Elsevier) pp 2278–91
[40] Zhang X, Grabowski B, Körmann F, Ruban A V, Gong Y, Reed R C, Hickel T and Neugebauer J 2018 Temperature dependence of the stacking-fault Gibbs energy for Al, Cu and Ni *Phys. Rev.* B **98** 224106
[41] Li X and Schönecker S 2017 First-principles prediction of the stacking fault energy of gold at finite temperature *Acta Mater.* **135** 88–95
[42] Wang Z Q and Beyerlein I J 2008 Stress orientation and relativistic effects on the separation of moving screw dislocations *Phys. Rev.* B **77** 184112
[43] Pellegrini Y-P 2018 Uniformly-moving non-singular dislocations with ellipsoidal core shape in anisotropic media *J. Micromech. Mol. Phys.* **3** 1840004
[44] Kim S, Kim H, Kang K and Kim S Y 2020 Relativistic effect inducing drag on fast-moving dislocation in discrete system *Int. J. Plast.* **126** 102629
[45] Eshelby J 1949 Uniformly moving dislocations *Proc. Phys. Soc.* A **62** 307
[46] Hirth J and Lothe J 1968 Interactions between moving dislocations *Dislocation Dynamics* ed A R Rosenfield, G T Hahn, A L Bement and R J Jaffee (McGraw-Hill)
[47] Weertman J 1962 Fast moving edge dislocations on the (111) plane in anisotropic face-centered-cubic crystals *J. Appl. Phys.* **33** 1631–5
[48] Blaschke D N 2019 Velocity dependent dislocation drag from phonon wind and crystal geometry *J. Phys. Chem. Solids* **124** 24–35
[49] Hunter A, Beyerlein I J, Germann T C and Koslowski M 2011 Influence of the stacking fault energy surface on partial dislocations in fcc metals with a three-dimensional phase field dislocations dynamics model *Phys. Rev.* B **84** 144108
[50] Hunter A, Zhang R F and Beyerlein I J 2014 The core structure of dislocations and their relationship to the material $\gamma$-surface *J. Appl. Phys.* **115** 134314
[51] Zhang X-C, Cao S, Zhang L-J, Yang R and Hu Q-M 2023 Unstable stacking fault energy and Peierls stress for evaluating slip system competition in body-centered cubic metals *J. Mater. Res. Technol.* **22** 3413–22